Finite Element Analysis Simulations for Ultrasonic Array NDE Inspections

Jeff Dobson[1, 2, a)], Andrew Tweedie[2], Gerald Harvey[2], Richard O'Leary[1], Anthony Mulholland[1], Katherine Tant[1] and Anthony Gachagan[1]

[1]*Centre for Ultrasonic Engineering, Department of Electronic & Electrical Engineering, University of Strathclyde, 204 George Street, Glasgow, G1 1XW, UK*
[2]*PZFlex, Weidlinger Associates Ltd., 50 Richmond Street, Glasgow G1 1XP, UK*

[a)]Corresponding author: jeff.dobson@strath.ac.uk

Abstract. Advances in manufacturing techniques and materials have led to an increase in the demand for reliable and robust inspection techniques to maintain safety critical features. The application of modelling methods to develop and evaluate inspections is becoming an essential tool for the NDE community. Current analytical methods are inadequate for simulation of arbitrary components and heterogeneous materials, such as anisotropic welds or composite structures. Finite element analysis software (FEA), such as PZFlex, can provide the ability to simulate the inspection of these arrangements, providing the ability to economically prototype and evaluate improved NDE methods. FEA is often seen as computationally expensive for ultrasound problems however, advances in computing power have made it a more viable tool. This paper aims to illustrate the capability of appropriate FEA to produce accurate simulations of ultrasonic array inspections – minimizing the requirement for expensive test-piece fabrication. Validation is afforded via corroboration of the FE derived and experimentally generated data sets for a test-block comprising 1D and 2D defects. The modelling approach is extended to consider the more troublesome aspects of heterogeneous materials where defect dimensions can be of the same length scale as the grain structure. The model is used to facilitate the implementation of new ultrasonic array inspection methods for such materials. This is exemplified by considering the simulation of ultrasonic NDE in a weld structure in order to assess new approaches to imaging such structures.

INTRODUCTION

Ultrasonic testing is one of the most commonly used methods in Non-Destructive Evaluation (NDE) and is one which greatly benefits from modelling throughout the inspection process. The use of modelling can provide a reduction of cost and time in the development and validation stages, through reduction of experimental test-cases, prototype fabrication and man-hours [1]. A wide variety of analytical and numerical techniques are available for modelling ultrasound. With both approaches, it is important that suitable validation is conducted to ensure confidence in the accuracy and reliability of the results.

The mathematical modelling technique Finite Element Analysis (FEA) [2-4] is now being used more frequently to model real systems due to its advantages over analytical modelling and recent advances in computing power. FEA can provide a much clearer understanding of the physical behavior of systems when compared to simple, constrained dimension analytical models [5]. Other benefits of FEA is the ability to model wave transmission, reflection and mode conversion [6], [7]. The software package used in this paper, PZFlex (Weidlinger Associates, Mountain View, California), is an explicit time-domain code [8], [9], which is extremely efficient for modelling complex NDE problems, including FMC inspections [10], and non-linear effects in bounded fields [11].

The use of ultrasonic phased arrays is increasing due to their improved inspection capability over single element transducers. One major advantage of an array is the ability to image the test structure at different locations from a single inspection location [12]. Moreover, the Full Matrix Capture (FMC) technique [13] has provided a useful tool for NDE array inspections with the ability to inspect large areas with high sensitivity. Corresponding processing using

the Total Focusing Method (TFM) [12] offers the capability to post-process FMC data and focus the transducer at every point in the test piece to generate an image.

The challenging nature of inspecting heterogeneous materials, such as anisotropic welds, is well known, due to their highly scattering nature [14, 15]. The varying orientation of grains in the microstructure of the weld causes scattering of the ultrasonic wave, leading to signal attenuation and undesirable beam steering/skewing. These internal reflections in the microstructure act as noise sources hence reducing the signal to noise ratio (SNR) of the inspection - compromising defect location and sizing capability. Accurate and reliable simulation tools are essential to aid in the development of these inspections. Analytical and semi-analytical methods of simulating heterogeneous materials can quickly reach their limit and so fully numerical analysis is required. Two dimensional FEA simulations have been proven to effectively simulate wave propagation through heterogeneous materials [10] but needs to be extended to three dimensions to provide a more accurate representation [16]. It is vital that these simulations are accurate and reliable through appropriate validation.

This paper describes work carried out to demonstrate the capability of FEA simulations for ultrasonic array NDE inspections. Validation of the modelling method is achieved via direct back to back corroboration between simulated and experimentally generated data for a homogeneous test block. The software code, PZFlex, is used to calculate computationally efficient 2D models to replicate a FMC inspection of a stainless steel calibration block and generate equivalent datasets. Images were then constructed using the TFM algorithm for both the experimental and numerical datasets. These images are then compared to demonstrate the accuracy of the simulations at predicting practical performance. A full 3D model was then simulated to indicate the ability to inspect volumetric defects and provide comparison between 2D and 3D simulations in terms of computational costs and result accuracy. The validated modelling approach is then used to consider the simulation of heterogeneous materials. These materials are more challenging to inspect due to their scattering nature, which is exemplified by considering the simulation of ultrasonic NDE in a weld structure.

VALIDATION OF THE MODELLING METHOD

Methodology

Experimental

The test block used for the experimental scans was a Harfang Microtechniques Inc. (Quebec City, Canada), Type B stainless steel calibration block designed for phased array transducers [17]. Included in this test block are numerous side drilled holes and four angled holes at varying angles as shown in Fig. 1. This calibration block is common throughout industry and provides good baseline evaluation of phased array transducers capability and performance.

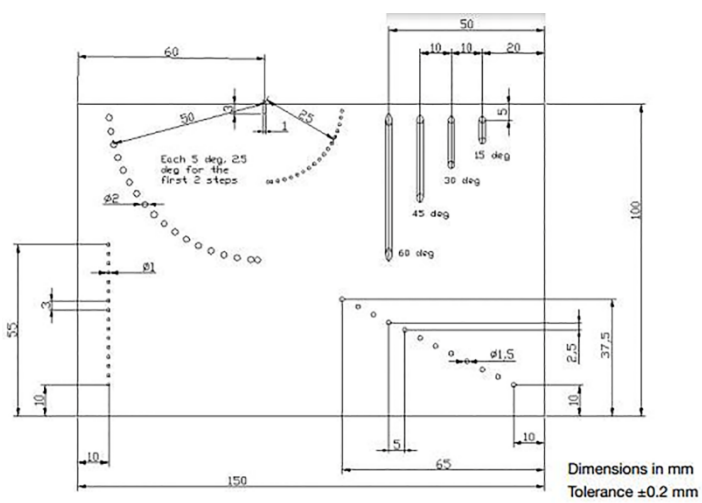

FIGURE 1. Schematic of Harfang Type B calibration block [17]

The ultrasonic scans were performed using a Vermon linear array transducer (Tours, France), with parameters as specified in Table 1. The transducer array excitation and data acquisition was afforded via a Zetec-Dynaray phased array controller (Quebec, Canada). FMC scans were conducted on four different positions on the calibration block as shown in Fig. 2.

TABLE 1. Phased array transducer specifications

Array Parameter	Value
Number of elements	128
Element pitch (mm)	0.75
Element length (mm)	12
Centre frequency (MHz)	2.25

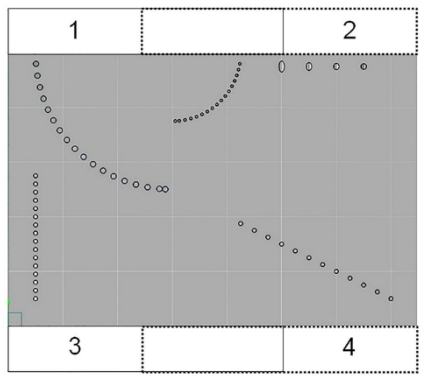

FIGURE 2. Schematic of test-piece indicating transducer array positions for FMC scans

2D Simulation

A 2D model was constructed in PZFlex to replicate the experimental scan as accurately as possible while remaining computationally efficient. Care has to be taken with this reduction in dimension due to the presence of angled holes which would require a full 3D model. In the first phase of modelling, the angled holes were omitted from the simulations.

The calibration block was constructed in PZFlex using the schematic shown previously in Fig. 1. The overall dimensions of the calibration block were used to create a region of stainless steel, with properties as shown in Table 2.The side drilled holes were then created by creating void regions of the correct size and location in the stainless steel region. In the void region, elements have zero density and stiffness, which is a good approximation for air due to its much lower acoustic impedance than steel.

TABLE 2. Stainless steel material properties

Stainless steel parameters	Value
Density (kgm^{-3})	7890
Longitudinal velocity (ms^{-1})	5620
Shear velocity (ms^{-1})	3100
Longitudinal attenuation (dB/m)	0.3
Shear attenuation (dB/m)	1.2

Further computational efficiency was achieved through only modelling the excitation of the calibration block with a pressure load to represent the transmitting transducer. This removes the requirement for the transducer structure and piezoelectric materials to be incorporated into the model, and allows for a (simplified yet representative) mechanical simulation. To provide an accurate simulation, an experimentally measured signal recorded from the transducer was

used as the input excitation to the model pressure source on the boundary. In order to acquire this signal, the transducer was placed on a solid stainless steel block and a pulse echo experiment was performed on each element to record the back wall reflections. A suitable back wall reflection was then truncated and saved for use as the input to the phased array transducer elements in the PZFlex simulations. The input pulse and its spectrum can be seen in Fig. 3. This input pulse was then applied as a pressure source on the model's boundary elements that represent the transducer array element. This meant that each array element was assumed to be identical, although each individual element's amplitude and phase could be varied if required.

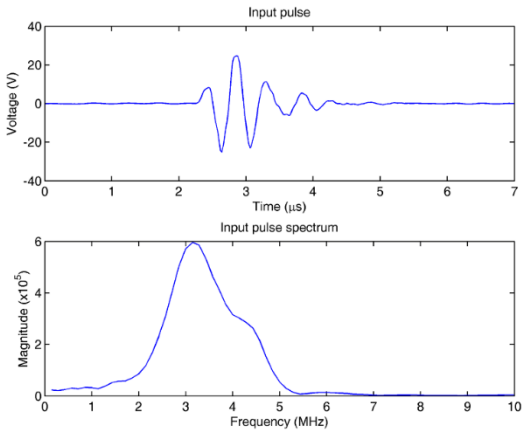

FIGURE 3. PZFlex model transducer input pulse

To generate the simulated FMC data, the A-scans for each transducer element must be recorded. The received echoes were recorded as the average time-variant, normal stress at each of the simulated array element locations. Each simulation generated 128 time traces to represent the signal received at each of the transducer elements. The simulation was run a total of 128 times with the input pulse applied to each of the transducer elements in turn to allow for the FMC dataset containing [128x128] time traces to be constructed.

The model was 2D plane strain and consisted of a structured Cartesian grid using quadrilateral elements. The model was meshed to give 15 elements per wavelength at 3.5MHz, giving the total number of elements used in the model as just over 1.3 million. A time stability factor of 0.95 was implemented to set the time step to 95% of its maximum value, which satisfies the Courant–Friedrichs–Lewy condition [18].

The simulations were run sequentially on a dual-core Dell Latitude laptop computer with each individual simulation taking approximately 4 minutes using 79MB of memory. This resulted in a total simulation time of 512 minutes to generate a single FMC dataset. Where suitable hardware is available, employing a parallel architecture could significantly reduce computation time by executing each simulation in parallel [19]. This gives the prospect of a total time of only 4 minutes to generate FMC data for a 128 element phased array transducer.

Results

The FMC datasets were processed in MATLAB (The MathWorks Inc., Natick, Massachusetts). TFM and a Hilbert transform were applied to the data to generate images, as shown in Figs. 4-7, for each array location illustrated in Fig. 2. All images were normalized to the maximum response amplitude of a central side drilled hole and are plotting on a dB scale. The same side drilled hole was used for both the experiment and simulation images for consistency. Each figure contains the (a) experimental and (b) simulation dataset at a particular location. The images are set up to show the area of the calibration block directly below the transducer when the transducer is positioned at 0 mm on the x-axis.

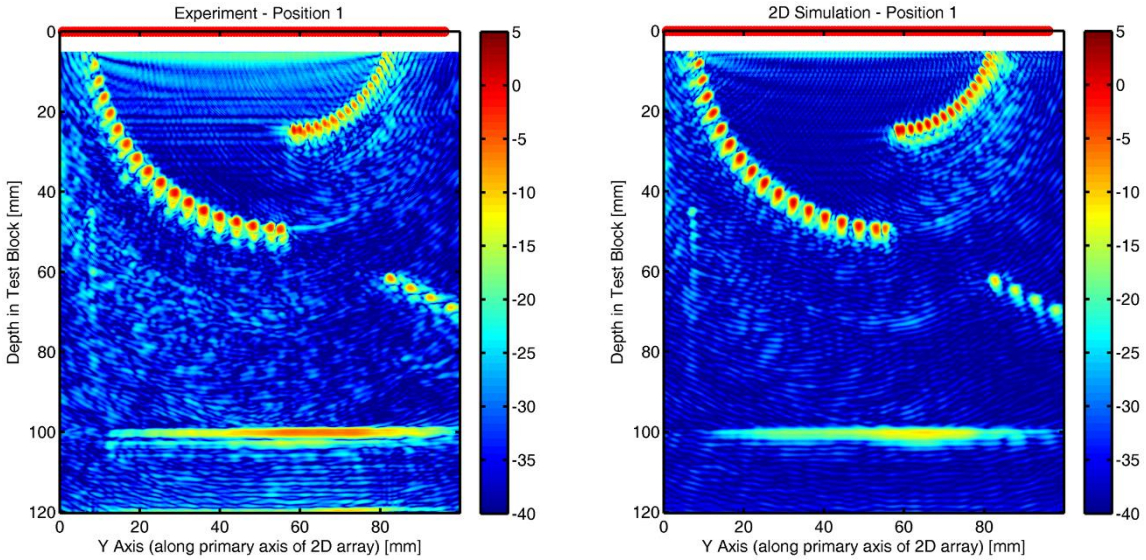

(a) (b)

FIGURE 4. TFM images for (a) experiment and (b) 2D simulation FMC datasets at array Position 1

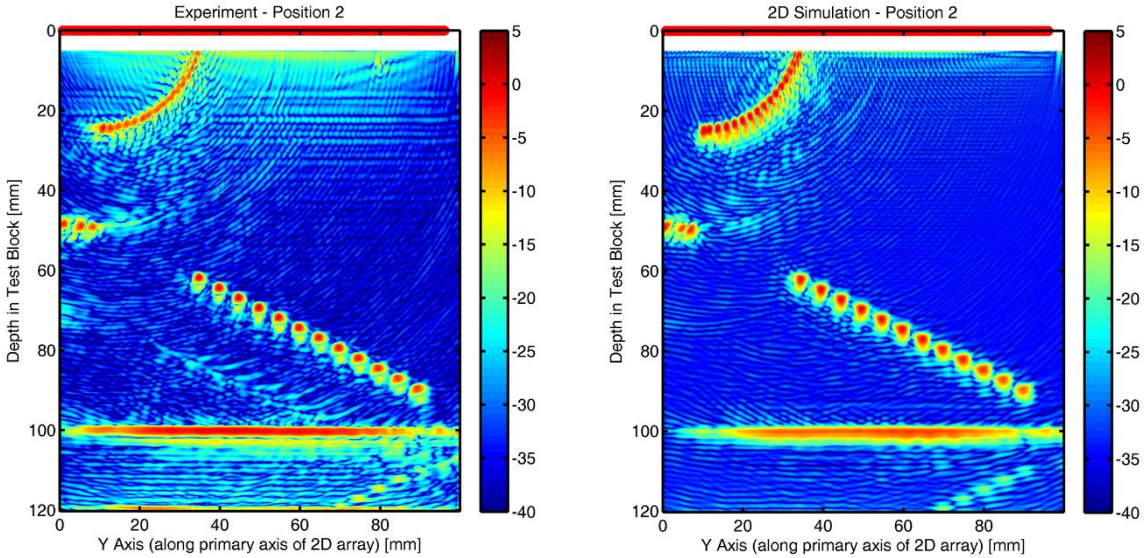

(a) (b)

FIGURE 5. TFM images for (a) experiment and (b) 2D simulation FMC datasets at array Position 2

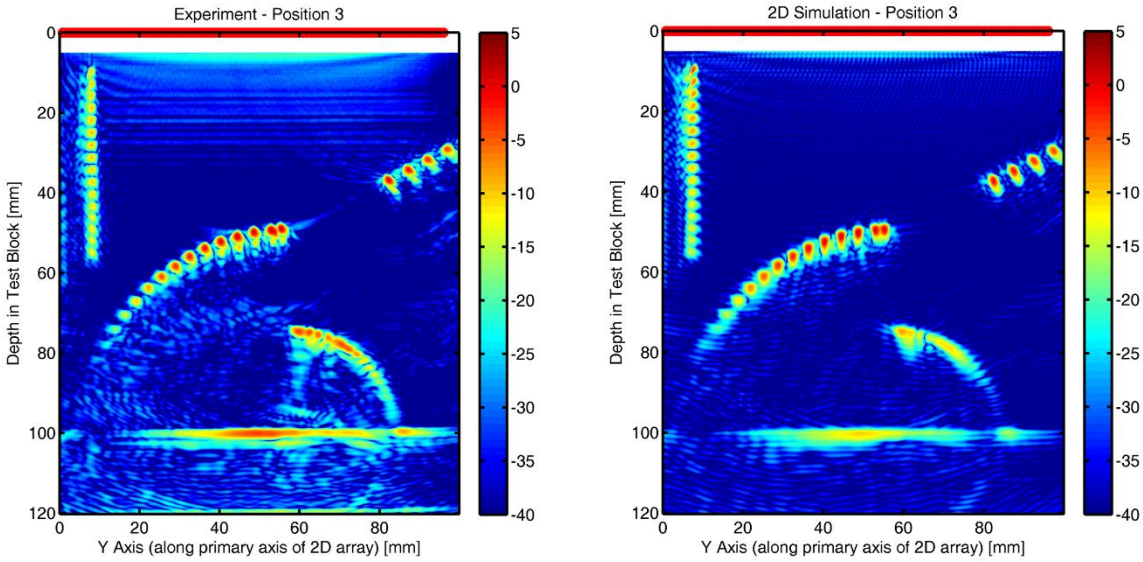

(a) (b)

FIGURE 6. TFM images for (a) experiment and (b) 2D simulation FMC datasets at array Position 3

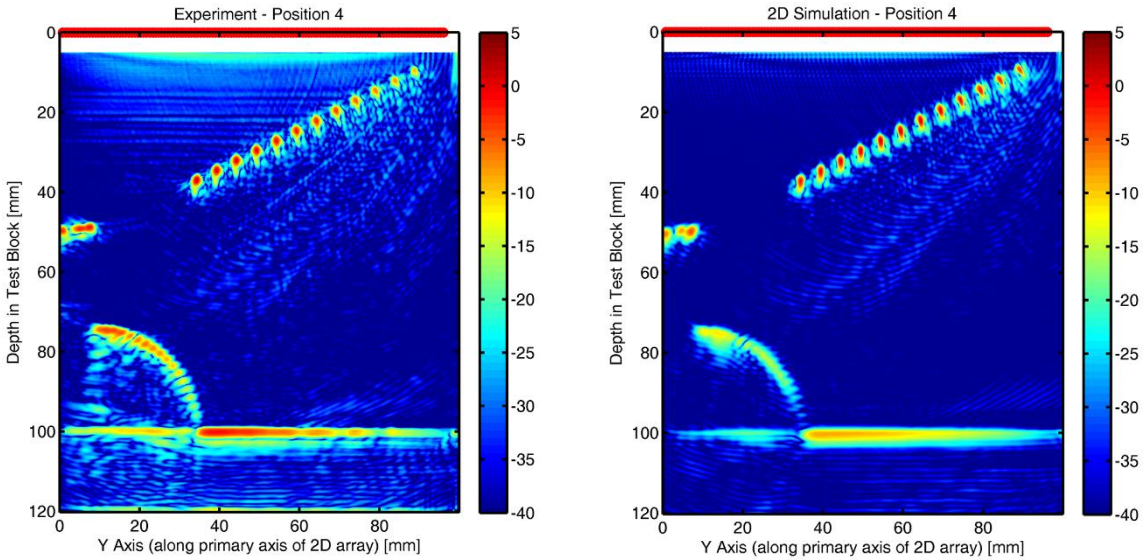

(a) (b)

FIGURE 7. TFM images for (a) experiment and (b) 2D simulation FMC datasets at array Position 4

Discussion

Simulation Performance

Evaluation of the TFM images shows excellent visual correlation between the simulated and experimentally generated datasets, with only slight differences in amplitude. The back wall location is correctly imaged at 100mm in each of the images. All of the defects present in the experimental images can be identified in the corresponding simulation dataset.

The data set acquired with the array at Position 2, shown in Fig. 5, has the transducer placed over the angled holes in the calibration block. In the experimental image, Fig. 5(a), one of these, at the shallowest angle, can be observed in the top right. This is not present in the corresponding simulation image as the defect was not present in the simulation.

In the experimental image, there are additional artefacts below the set of holes near the back wall. It is believed that these are due to secondary effects from the scattering of the input wave with the angled holes.

To provide a quantitative comparison, the angled series of 12 side drilled holes near the back wall in Position 2 were used to determine the positioning accuracy of the results. The center of the holes was determined by taking the maximum amplitude of the TFM image for each hole. The resulting depths, Table 3, and horizontal positioning of the holes, Table 4, are presented along with the actual values from the schematic for reference. The holes are numbered with 1 being the top left and 12 the bottom right as seen in Fig. 5. It should be noted that the pixel size of all TFM images is 0.05mm.

TABLE 3. Depth of angled series of side drilled holes in Position 2

Hole number	Actual depth (±0.2 mm)	Experiment depth (±0.025 mm)	2D simulation depth (±0.025 mm)
1	62.5	61.7	61.95
2	65	64.25	64.45
3	67.5	66.7	66.95
4	70	69.2	69.4
5	72.5	71.65	71.9
6	75	74.2	74.4
7	77.5	76.7	76.9
8	80	79.3	79.35
9	82.5	81.8	81.9
10	85	84.4	84.45
11	87.5	86.95	86.9
12	90	89.5	89.45

TABLE 4. Horizontal positioning of angled series of side drilled holes in Position 2

Hole number	Actual horizontal position (±0.2 mm)	Experiment horizontal position (±0.025 mm)	2D simulation horizontal position (±0.025 mm)
1	34.375	34.7	34.4
2	39.375	39.7	39.45
3	44.375	44.65	44.45
4	49.375	49.65	49.45
5	54.375	54.65	54.5
6	59.375	59.65	59.6
7	64.375	64.6	64.65
8	69.375	69.6	69.7
9	74.375	74.5	74.75
10	79.375	79.35	79.8
11	84.375	84.3	84.7
12	89.375	89.25	89.8

The results from the depth positioning provide good corroboration between experimental and FE derived datasets, with an average difference of 0.15mm and maximum difference of 0.25mm. There is also good correlation between

the experiment and FE derived datasets for the determination of the horizontal positioning of the series of holes, where there is an average difference of 0.24mm and a maximum difference of 0.55mm. This confirms that the simulations can accurately predict the experimental data.

Full 3D model

A 3D model was constructed to simulate the effects of inspecting over the angled holes. This would give a better representation of the inspection but at a cost of a much larger and computationally demanding model. A CAD geometry of the calibration block was created in Midas NFX (Midas, Seoul, Korea) using the manufacturers design specifications, as illustrated in Fig. 8, and imported directly into PZFlex.

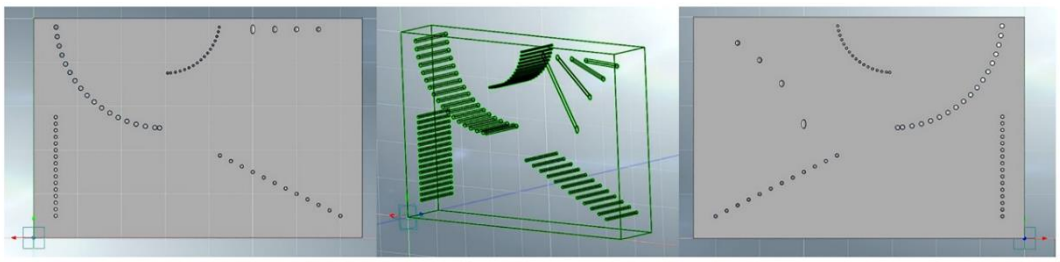

FIGURE 8. Calibration block CAD file

The model was meshed at a lower frequency of 2.25MHz, which reduced computation costs considerably, resulting in an 87 million element model. The rest of the simulation parameters were replicated from the 2D model previously described. The input pulse and received signals were the same as used previously, but were now applied and recorded over a 2D area representing each array element location.

The 3D model was run on the same laptop, requiring 7.2GB of memory and a run time of 5 hours. This made the computational time required to sequentially generate the FMC dataset very large. Options are available to reduce this through parallelization with a Message Passing Interface (MPI) [20], which was seen to reduce a single run by five times, using PZFlexCloud [19]. The simulations on PZFlexCloud, produced a FMC dataset for a full 3D model in 5 hours. The resulting TFM image can be seen in Fig. 9 along with the corresponding experimental result.

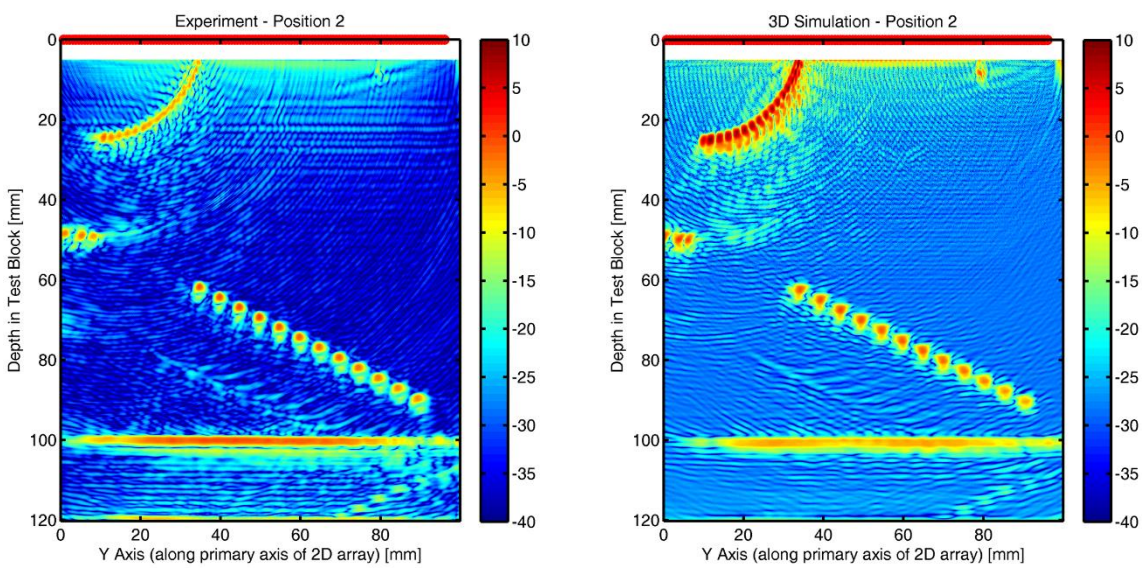

(a) (b)

FIGURE 9. TFM images for (a) experiment and (b) 3D simulation FMC datasets at Position 2

As with the 2D model, the 3D model was successful in recreating all of the defects seen in the experimental results. However, despite the greatly increased computational cost of the 3D Model, simulation results are in general similar to those produced by the 2D model. This demonstrates the benefit of reducing the model to 2D when possible for improved computational efficiency.

In addition, the 3D results display some features which are not present in the 2D data set. The angled hole at the top right of the block can be seen in both the 3D and experimental images (79mm along y-axis at 8mm depth). The artefacts below the side drilled holes near the back wall have also been replicated in the simulation, highlighting the capability of 3D models to produce a complete representation of the practical inspection.

There is higher background noise present in the simulation which is due to the presence of under meshed shear waves. This could be prevented and improve the simulation result by increasing the meshing of the model, however this will greatly increase the computation costs.

HETEROGENEOUS MATERIAL MODELLING

Methodology

To accurately simulate inspections using FEA, it is essential to have an accurate knowledge of material properties and structure. For anisotropic welds, this means a sufficient knowledge of grain boundaries and elastic stiffness are required. An effective technique to quantify anisotropic weld microstructure is Electron Back-Scatter Diffraction (EBSD) [21]. This technique can map the micro texture of the crystalline materials and also determine the crystallographic orientation, which can then be implemented in a capable FEA model.

This work builds on previous work done by Harvey et al [10] to accurately simulate ultrasonic inspections of an anisotropic weld described by Carpentier et al [21]. The weld map generated by the EBSD, Fig. 10, illustrates the grain boundaries of the 11 dominant grain orientations, Table 5. The resolution of the EBSD scan was within the Rayleigh scattering domain and the grain orientations with a difference of 20° or less are grouped to the dominant orientation. The calculated stiffness constants for the weld are C_{11} = 230.6GPa, C_{12} = 133.5GPa and C_{44} = 129.8GPa [22].

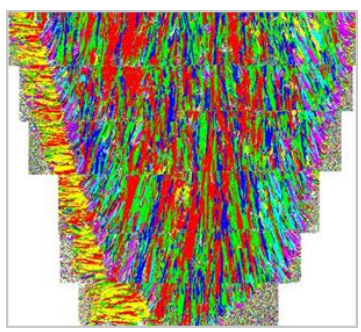

FIGURE 10. Map of weld where each color represents one of 11 dominant grain orientations. Figure reproduced from 'Evaluation of a new approach for the inspection of austenitic dissimilar welds using ultrasound phased array techniques' by C. Carpentier, C. Nageswaran and Yau Yau Tse, published in the proceedings of the 10th European Conference on Non-Destructive Testing (ECNDT), vol. 1, 2010, ISBN 9781617827914, and appears here with the kind permission of the European Federation for NDT (EFNDT) and the authors.

TABLE 5. Dominant grain orientations expressed as rotation angles [21]

Color	α – Rotation about x (°)	β – rotation about y (°)	λ – rotation about z (°)
Red	0	0	0
Lime green	176.1	195.4	352.3
Yellow	331.5	4.9	255.8
Blue	355.3	43.7	272.2
Fuchsia	5.1	6.0	322.3
Cyan	200.5	221	326
Brown	197.7	196.3	235.8
Purple	32.8	23.0	329.4
Grey	338.6	24.8	257.0
Green	36.4	18.5	353.5
White	342.9	40	300.6

From the EBSD data, a file was constructed which could be imported into PZFlex to provide accurate reconstruction of the weld in the model. The material file for the simulations contained each dominant orientation color and this information is used within the software to rotate the stiffness matrix to generate the required orientation. This produced unique material properties for the colours allowing for the heterogeneity of the weld to be simulated.

The model was constructed to perform FMC inspections with an array transducer directly coupled over the weld with stainless steel either side. To illustrate the feasibility of using FEA simulations to investigate numerous parameters quickly, simulations were done for varying frequencies and array aperture length. It was demonstrated in [10] that the through transmission spectra of the weld structure is highly frequency dependent and above 1.5 MHz the SNR was inadequate. Therefore, selected frequencies to investigate were identified as 0.5, 1.0 and 1.5MHz - each simulated array layout satisfied the half wavelength (λ/2) spatial sampling criterion in order to prevent grating lobes. The number of elements was then varied to produce arrays equal in length to: half weld width; weld width; and one and a half times weld width. The arrays were positioned at the center of the weld and the width of the weld at the surface was ~90mm. Table 6 contains the complete list of simulations run and each of their respective array parameters. The 9 simulations were then repeated to include a side drilled hole to act as a defect. The side drilled hole was positioned centrally in the weld and had a diameter of 1mm.

TABLE 6. Simulation parameters for anisotropic weld study

Simulation number	Frequency (MHz)	Element Pitch (mm)	Array length (mm)	Number of array elements
1	0.5	5.92	47.36	8
2	0.5	5.92	94.72	16
3	0.5	5.92	142.08	24
4	1.0	2.96	44.4	15
5	1.0	2.96	88.8	30
6	1.0	2.96	133.2	45
7	1.5	1.97	45.31	23
8	1.5	1.97	90.62	46
9	1.5	1.97	135.93	69

The validated modelling approach previously discussed was extended to include the simulation of the weld micro structure. As before, the transducer representation was simplified, with a pressure load applied to the surface which was represented as a wavelet input at the required central frequency. The application of the pressure load and the approach of generating the FMC data by calculating the average normal stress at each element location was kept the same. Similarly to the previous work described earlier in this paper, an experimentally collected signal could be used

to provide a more realistic representation. The model was again 2D plane strain and consisted of a structured Cartesian grid using quadrilateral elements. The element size was calculated to provide 15 elements per wavelength for the shortest wavelength propagating in the model. The shortest wavelength was calculated from the shear velocity in the steel and the excitation frequency. Table 7 contains information on the number of elements in each simulation along with the individual simulation run time and time to generate the FMC date. The time stability factor was again set to 0.95 to satisfy the Courant–Friedrichs–Lewy condition [18].

TABLE 7. Simulations model and run time details

Simulation number	Meshing frequency (MHz)	Number of model elements (x e^3)	Individual run time (seconds)	Total FMC time (minutes)
1	1.0	394	~30	4
2	1.0	394	~30	8
3	1.0	578	~40	16
4	1.0	394	~30	7.5
5	1.0	394	~30	15
6	1.0	578	~40	30
7	1.5	905	~90	34.5
8	1.5	905	~90	69
9	1.5	1276	~120	138

Results

The FMC data sets were processed in MATLAB as before and the TFM and Hilbert transform were applied to generate the resultant images. Figures 11, 12 and 13 contain the images from simulations with an array aperture equal to 0.5, 1 and 1.5 of the weld width respectively and no defect present in the weld. Figures 14, 15 and 16 contain the images from simulations with the array aperture length equal to 0.5, 1 and 1.5 of the weld width respectively but this time with a defect present in the weld. Each figure contains three image results from the different simulation frequencies.

All images were normalised to the maximum response in the image and are plotted on a dB scale. The TFM algorithm assumed a single homogenized wave speed in the image reconstruction. This means some accuracy in image reconstruction is lost due to local variations in the wave speed within the weld, although techniques exist to counter this, such as time reversal acoustics [10] and DORT [23]. The images are set up to show the area of the calibration block directly below the transducer with the transducer positioned at 0 mm on the x-axis.

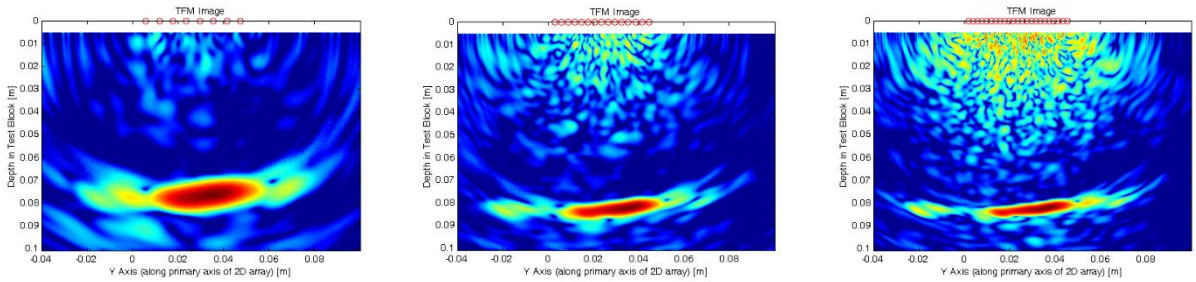

(a) (b) (c)

FIGURE 11. FE derived TFM images of the weld structure in the absence of any defect where the array aperture is equal to 0.5 of weld width: (a) 0.5 MHz, (b) 1.0MHz and (c) 1.5MHz

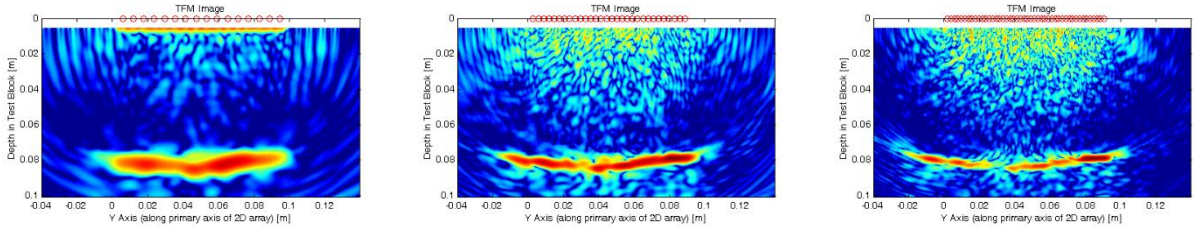

(a) (b) (c)

FIGURE 12. FE derived TFM images of the weld structure in the absence of any defect where the array aperture is equal to the weld width: (a) 0.5 MHz, (b) 1.0MHz and (c) 1.5MHz

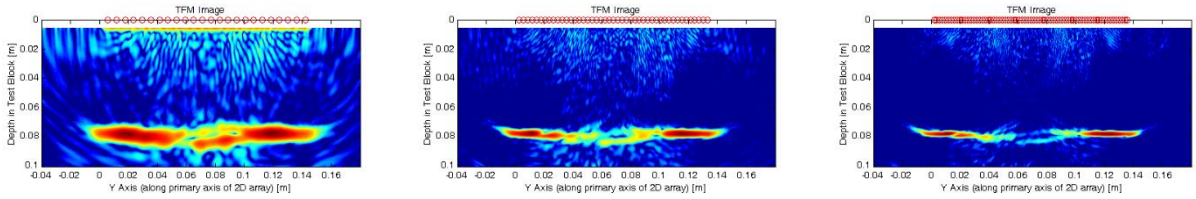

(a) (b) (c)

FIGURE 13. FE derived TFM images of the weld structure in the absence of any defect where the array aperture is equal 1.5 of weld width: (a) 0.5 MHz, (b) 1.0MHz and (c) 1.5MHz

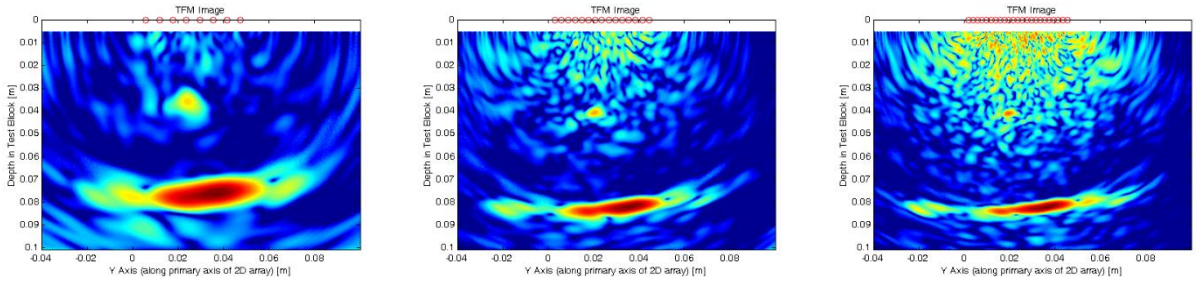

(a) (b) (c)

FIGURE 14. FE derived TFM images of the weld structure in the presence of a defect where the array aperture is equal 0.5 of weld width: (a) 0.5 MHz, (b) 1.0MHz and (c) 1.5MHz

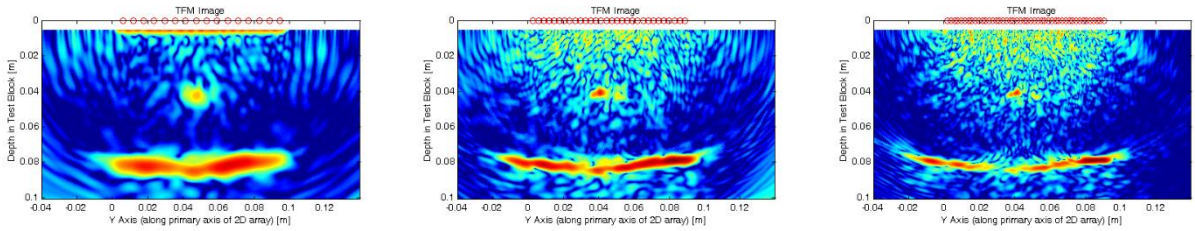

(a) (b) (c)

FIGURE 15. FE derived TFM images of the weld structure in the presence of a defect where the array aperture is equal to weld width: (a) 0.5 MHz, (b) 1.0MHz and (c) 1.5MHz

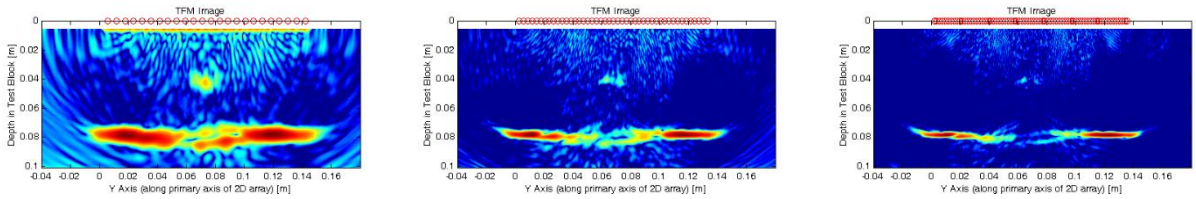

(a) (b) (c)

FIGURE 16. FE derived TFM images of the weld structure in the presence of a defect where the array aperture is equal to 1.5 of weld width: (a) 0.5 MHz, (b) 1.0MHz and (c) 1.5MHz

Discussion

These results highlight the frequency dependence of weld inspection and the noise caused from back scatter due to the grain structure. It is clear to see that as the inspection frequency increases, the level of back scatter increases due to the smaller wavelength reflecting more from grain boundaries.

The feasibility of simulations has been clearly illustrated, allowing fast and efficient simulations of heterogeneous material inspections. This allows for multiple parameters to be investigated without the need to manufacture multiple prototype test pieces or transducer probes.

While these 2D FEA simulations provide a good approach to modelling the inspection of anisotropic welds the progression to full 3D models is required. Grain structures are a volumetric feature which is better represented in 3D and so a 3D simulation will provide a more representative simulation. Furthermore, each weld, even along a single weld length, is unique and does not contain the same microstructure. A suitable method to allow for these differences would be to statistically generate volumetric data sets from real weld data. The simulation of inspections done in 3D could then be evaluated against 2D results to investigate their similarities and differences.

CONCLUSIONS AND FUTURE WORK

A validated finite element analysis modelling approach has been developed for the simulation of heterogeneous materials. Validation was achieved through the corroboration between simulation results with experimentally generated data sets for an ultrasonic phased array inspection of a homogeneous calibration block. Extending this modelling approach to consider the more challenging heterogeneous materials was demonstrated by simulating ultrasonic inspections of an anisotropic weld. The feasibility of finite element analysis modelling to quickly and accurately model these inspections has been illustrated – minimizing the requirement for expensive test piece fabrication. Future work includes comprehensive analysis of weld inspection results and extending to simulate weld inspections in 3D.

ACKNOWLEDGEMENTS

Funding from the Engineering and Physical Sciences Research Council for an Engineering Doctorate studentship is gratefully acknowledged (Grant no. EP/I017704/1), as is financial, technical and practical support by Weidlinger Associates Ltd, the University of Strathclyde and the wider UK Research Centre in NDE.

REFERENCES

1. A. Quarteroni, Notices of the AMS **56**, 10-19 (2009)
2. O. C. Zienkiewicz and R. L. Taylor, *The Finite Element Method* (Butterworth-Heinemann, Oxford, UK, 2000).

3. T. K Helen and A. A. Becker, *Finite Element Analysis for Engineers: A Primer* (NAFEMS, Hamilton, UK, 2013).
4. D. V. Hutton and J. Wu, *Fundamentals of finite element analysis*, (McGraw-Hill, New York, USA, 2004).
5. C. Desilets, G. Wojcik, L. Nikodym and K. Mesterton, "Analyses and measurements of acoustically matched, air-coupled tonpilz transducers" in *Ultrasonics symposium 1999*, (IEEE International, Nevada, 1999), pp. 1045-1048.
6. D. N, Alleyne and P. Crawley, IEEE Transactions on Ultrasonics, Ferroelectrics, and Frequency Control **39**, 381-397, 1992.
7. M. J. S. Lowe, D. N. Allen and P. Crawley, Journal of Applied Mechanics **65**, 649-656, (1998).
8. G. Wojcik, D. Vaughan, V. Murray and J. Mould Jr, "Time-domain modeling of composite arrays for underwater imaging", in *Ultrasonics symposium 1994*, (IEEE International, Cannes, 1994), p. 1027-32.
9. G. Wojcik, D. Vaughan, N. Abboud and J. Mould, "Electromechanical Modeling Using Explicit Time-Domain Finite-Elements" in: *Ultrasonics symposium 1993*, (IEEE International, Baltimore, 1993), p. 1107-12.
10. G. Harvey, A. Tweedie, C. Carpentier, P. Reynolds, "Finite Element Analysis of Ultrasonic Phased ArrayInspections on Anisotropic Welds" in *Review of Progress in Quantitative Nondestructive Evaluation*, eds. D. O.Thompson and D. E. Chimenti, (American Institute of Physics, 1335, Melville, NY), **30,** 827-834 (2010).
11. G. Harvey and A. Gachagan, IEEE Transactions on Ultrasonics, Ferroelectrics, and Frequency Control **58**, 808-819, (2011).
12. B. W. Drinkwater and Wilcox P. D, NDT&E International **39**, 525-541, (2006).
13. C. Holmes, B. W. Drinkwater and P. D. Wilcox, NDT&E International **38**, 701-711, (2005).
14. J. R. Tomlinson, A. R. Wagg and M. J. Whittle, British journal of non-destructive testing **24**, 119-124, (1980).
15. I. N. Ermolov, and B. P. Pilin, NDT&E International **9**, 275-280, (1976).
16. A. Lhémery, P. Calmon, I. Lecœur-Taïbi, R. Raillon and L. Paradis, NDT&E International **33**, 499-513, (2000).
17. Harfang Microtechniques Inc., Characterisation Block Product Specifications. 2006.
18. R. Courant, K. Friedrichs and H. Lewy. IBM journal of Research and Development **11**, 215-234, (1967).
19. R. O'Leary, G. Brown and G. Harvey, "Droplets, vapours and clouds – a new approach to capacitive transducer manufacture", in *Ultrasonics symposium 2013*, (IEEE International, Prague, 2013), pp. 1105-1108.
20. W. Gropp, E. Lusk, N. Doss and A. Skjellum, Parallel computing 22, 789-828, (1996).
21. C. Carpentier, C. Nageswaran and Y. Y. Tse, "Evaluation of a new approach for the inspection of austenitic dissimilar welds using ultrasonic phased array techniques", in *Proc 10th ECNDT conference*, (ECNDT, Moscow, 2010), pp. 442-444.
22. A Juva and J. Lenkkeri, "The effect of anisotropy on the propagation of ultrasonic waves in austenitic stainless steel", in *CSNI specialist meeting on Reliability of Ultrasonic Inspection of Austenitic Material*s, (CSNI, Belgium, 1980), pp. 2-24.
23. C. Prada, S. Manneville, D. Spoliansky and M. Fink, The Journal of the Acoustical Society of America **99**, 2067-2076 (1996).